

Direct-expansion solar-assisted heat pump coupled with crystallisation-controlled supercooled PCM for shifting building electricity demand

Cagri Kutlu^{a,*}, Yanan Zhang^a, Qinghua Lyu^b, Yuehong Su^a, Saffa Riffat^a

^a Department of Architecture and Built Environment, University of Nottingham, University Park NG7 2RD, UK

^b School of Science, Hubei University of Technology, Hubei, Wuhan, China

ARTICLE INFO

Keywords:

Demand-shifting
Direct-expansion solar-assisted heat pump (DX-SAHP)
Crystallisation controllable
Phase change material (PCM)

ABSTRACT

This paper proposes a novel approach for improving the performance of a direct-expansion solar-assisted heat pump (DX-SAHP) system by integrating a crystallisation controllable phase change material (PCM) and building energy demand shifting strategy. The proposed system aims to reduce buildings' energy consumption while utilizing solar energy efficiently. Sodium acetate trihydrate (SAT) as the crystallisation controllable supercooled PCM has a promising feature of releasing the stored latent heat when it is externally triggered, allowing the user to control the stored heat whenever needed. In the study, the PCM can store the thermal energy generated by the DX-SAHP during peak solar hours in an efficient way. This stored energy can be released when solar energy is unavailable, but the heating is requested. This approach not only reduces the load on the heat pump system but also makes efficient use of the stored thermal energy by crystallisation controllable PCM. A detailed controlling methodology of the system is given, and heating output is controlled considering the level of solar irradiance. The proposed system was modelled and simulated using MATLAB, and the results show that the integration of crystallisation controllable PCM and building demand shifting strategy can significantly reduce the energy consumption of the buildings. On the low solar radiation day, the COP improvement compared to the air source heat pump system was found 9.4%, this improvement value can reach 77% on high solar radiation days. The system can also effectively utilize solar energy and reduce the overall carbon footprint of buildings.

1. Introduction

The mitigation of climate change still poses a significant challenge despite massive efforts to address this issue. To effectively implement climate change policy and meet the objectives of European environmental policy, it is crucial to lower the contribution of all sectors to greenhouse gas (GHG) emissions [1]. It is absolutely essential to reduce GHG emissions in the residential sector as well. The heating demand in residential and commercial buildings has increased significantly [2] and it rises greenhouse gas emissions together with concerns about the environment. In 2021, households represented 27.4 % of final energy consumption in European Union and, 77.8 % of residential energy consumption was used for space heating and domestic hot water (DHW) needs [3]. As a result, there is a growing interest in developing energy-efficient and sustainable solutions for space heating and DHW applications.

There is a significant effort to increase use of heat pumps (HP) in built environments instead of gas boiler to reduce carbon emissions. However, the performance of conventional air source HP is still a question for end users, especially in cold areas, because its performance depends on the ambient temperature and its performance suffers considerably. Therefore, various renewable heat sources have been integrated on heating systems [4] such as ground source heat pumps [5] and solar assisted heat pumps [6]. As it is in the scope of this study, solar assisted heat pumps have been introduced and developed for a long time for higher performance using available solar energy. In this way, electricity consumption can be reduced [7]. However, because of the nature of the solar energy, there will be a mismatch between available solar energy and building heating demand. The system requires an additional thermal storage to supply higher heat source than ambient air. It is called indirect solar assisted heat pump systems and many papers have investigated it in detail [8]. Dik et al., [9] presented that using indirect solar assisted heat pump can reduce the energy consumption around

* Corresponding author.

E-mail address: cagri.kutlu2@nottingham.ac.uk (C. Kutlu).

Nomenclature		ϕ	PCM liquid fraction
A_{col}	Collector area, m ²	Subscripts	
c_1	Heat loss term, W m ⁻² K ⁻¹	am	Ambient
c_2	Heat loss term, W m ⁻² K ⁻²	col	Collector
c_p	Specific heat, J kg ⁻¹ K ⁻¹	comp	Compressor
D	Diameter, m	cond	Condenser
G	Solar irradiance, Wm ⁻²	dis	Discharge
h	Specific enthalpy, J kg ⁻¹	htf	Heat transfer fluid
L	Heat of fusion, kJ kg ⁻¹	is	Isentropic
\dot{m}	Mass flow rate, kg s ⁻¹	r	Refrigerant
M	Mass, kg	st	Storage
Nu	Nusselt number	suc	Suction
P	Pressure, kPa	n	Node number
Pr	Prandtl number	w	Water
Ra	Rayleigh number	t	Tank
\dot{Q}	Heat rate, W	Abbreviations	
T	Temperature, °C	COP	Coefficient of performance
U	Overall heat transfer coefficient, W m ⁻² K ⁻¹	DHW	Domestic hot water
V	Volume, m ³	HP	Heat pump
Greek letters		PCM	Phase change material
η	Efficiency	LHTES	Latent heat thermal energy storage
ρ	Density, kg m ⁻³	SAT	Sodium acetate trihydrate

41.5 % in an average day compared to conventional air source heat pumps. However, in order to avoid indirect HP's heat exchanger losses, buffer tank heat losses and bulky space of the buffer tank, direct-expansion solar-assisted heat pump (DX-SAHP) was introduced. In this system, refrigerant is circulated directly inside the solar collector, and it is evaporated in the collector with solar energy. The studies about the DX-SAHP have focused on bare collectors in order to benefit both solar energy and available air energy. Chow et al., [10] used weather data of Hong Kong in their study and they found that the DX-SAHP system could achieve a year-long average COP of 6.46 which was significantly higher than conventional air source HP systems. Rodrigues et al., [11] tested the DX-SAHP in extreme conditions and reported that COP varies between 1.9 and 2.7. Even the collector is covered by snow, the condenser heating load reached 1.5 kW with condensing temperature of 32 °C. The effect of condenser area and refrigerant charging were also investigated [12]. The studies also revealed that the performance of the DX-SAHP is mainly influenced by solar radiation intensity. Kong et al., [13] presented a modelling work using R410a refrigerant for water heating purpose. They concluded that when solar radiation intensity increases from 300 W/m² to 900 W/m², water heating time decreases by 32.8 % and average COP increases by 46.3 %. It is obvious that solar irradiance improves performance and increases the heating capacity, the important issue here is the controlling the system operation considering varying solar radiation intensity. Kong et al., [14] applied a control strategy of the DX-SAHP operation and set experiments. Their control strategy was regulating the degree of superheating 5–10 °C by controlling the expansion valve opening area. Rabelo et al., [15] tested valve opening of the small scale CO₂ charged DX-SAHP unit. They presented that controlling the expansion valve opening can provide maximum COP of the system. Rabelo et al., [16] also investigated a transcritical CO₂ DX-SAHP system to control refrigerant flow rate by using needle expansion valve. They presented a new correlation based on experimental data for the mass flow rate of the working fluid. Yin et al., [17] carried out an experimental study to predict evaporation temperature based on environmental parameters. They used independent variables as solar radiation, ambient temperature and wind speed, and predicted the evaporation temperature using linear regression method. It was reported that solar radiation intensity has significant influence on evaporation temperature.

In addition to DX-SAHP, latent heat storage is also an emerging technology that can provide more efficient, space and cost-effective way to store thermal energy for heating. Phase change materials (PCMs), which have a high latent heat capacity and can store and release thermal energy at a constant temperature during the phase change process have been used as storage material. This makes it a suitable option for storing thermal energy for demand shifting purposes to promote renewable energy sources [18]. Latent heat storage unit can provide heat to the evaporator of the heat pump thus, a higher heat source temperature can be provided [19]. Recently, Zhu et al., [20] presented simulation and experiment results of solar evaporative heat pump system integrated with a PCM tank between the heat pump evaporator and solar collector. Their findings indicated that daily energy consumption of the heat pump with PCM is only 41.2 % of the single heat pump heating system. Another configuration of solar assisted heat pump with PCM unit is replacing the PCM storage unit between the building and condenser of the heat pump. This configuration also serves the demand shifting as the heat pump operates during off peak hours and charges the PCM storage [21–23]. However, heat losses of the conventional PCM systems can be a problem since the PCM loses heat and low temperature PCM could be useless for heating applications. Supercooled PCMs solve this problem, the latent heat is only released when the PCM is triggered to induce crystallisation which makes it suitable for load shifting and synchronising the available solar heat and demand issue in building heating systems [24]. There are many methods to trigger a controlled crystallization to release the latent heat of the most commonly used PCM sodium acetate trihydrate (SAT) [25]. In order to trigger the stored latent heat, step motor injection was designed [26], Peltier devices were used [27] and electric triggering devices were prepared [28], and applied to building heating systems [24,29].

The use of DX-SAHP and heat storage also address to demand shifting concept. Demand shifting is a strategy that aims to move energy consumption from peak periods to off-peak periods, in order to reduce energy costs and stress on the grid. It is also important in order to reduce carbon emissions, because emissions from the grid reach peak level during peak demand periods because of fossil-based electricity generation [30].

Therefore, this paper proposes a system integrating DX-SAHP, LHS, and demand shifting for space heating and DHW applications. The

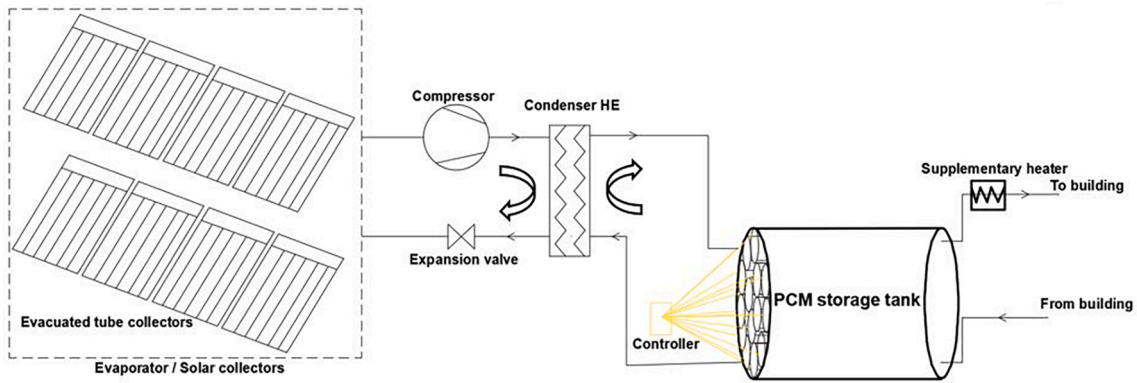


Fig. 1. Schematic of a DX-SAHP coupled with crystallisation controllable supercooled PCM storage tank.

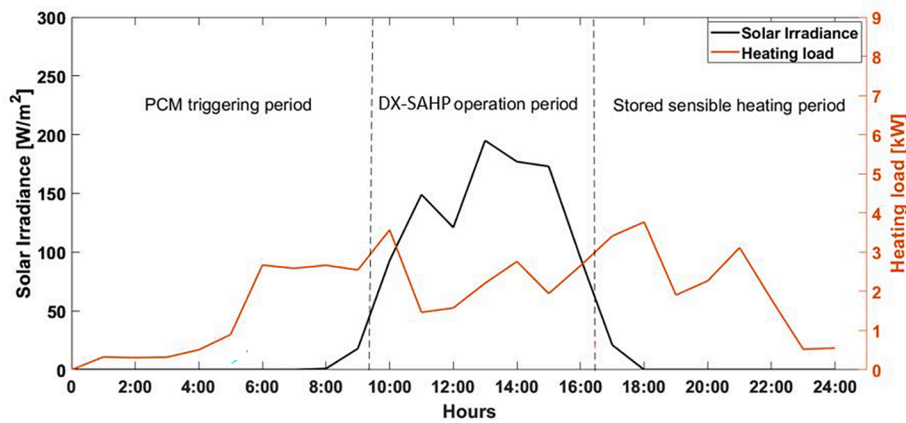


Fig. 2. Proposed system operation periods.

proposed system aims to provide an efficient and sustainable solution while reducing energy consumption, promoting solar energy and balancing the electricity grid. The system will be evaluated using a simulation model that considers control strategies, energy demand of the building and weather conditions. The main objectives of this paper are as follows:

- **Design and Develop an Efficient and Sustainable DX-SAHP System:** The primary aim of this research is to propose and develop a DX-SAHP system that emphasizes energy efficiency and reduced energy consumption. To achieve this objective, the system incorporates evacuated tube collectors, which have been underutilized in the literature [31,32]. Unlike conventional bare/unglazed solar collectors, the evacuated tube collectors demonstrate superior performance in cold and low solar radiation areas/seasons. By adopting evacuated tube collectors, the system can overcome the negative impact of cold weather conditions and function optimally day and night. This approach not only ensures efficient energy utilization but also promotes the system's ability to relieve grid stress by operating only during the off-peak times.
- **Evaluate the Proposed System Using a Comprehensive Simulation Model:** To assess the effectiveness and performance of the proposed DX-SAHP system, a detailed simulation model is employed. This simulation considers various control strategies, the energy demand profile of the building, and real weather conditions. Previous studies have highlighted the necessity of considering real weather data and building heating demand profiles in evaluations of DX-SAHP systems. By incorporating these factors into our transient simulations, we can provide a more realistic and accurate assessment of the system's performance under different scenarios.

- **Develop Solar Profile-based Heating and Performance Maps for Control Methodology:** In this study, solar profile-based heating and performance maps are developed to establish a robust control methodology for the DX-SAHP system. These are derived from extensive performance predictions, providing valuable insights into the system's behavior under varying solar energy availability and building heating demands. Implementing the control methodology based on these findings will contribute to the system's efficiency and overall performance, ensuring optimal energy utilization.
- **Demonstrate the Effectiveness of Supercooled PCMs in the DX-SAHP Unit:** To highlight the system's energy efficiency, cost-saving potential, and positive environmental impact, this research introduces the use of supercooled PCMs in the DX-SAHP unit. The incorporation of supercooled PCMs in the DX-SAHP represents a novel and innovative approach, demonstrating their effectiveness in improving the system's performance and reducing environmental impact. Through comprehensive simulations, the benefits and advantages of using supercooled PCMs will be demonstrated and compared to conventional air source heat pump system.

2. System components and methodology

The system consists of three main sections namely, solar collectors, heat pump and a PCM storage tank. Evacuated tube solar collectors work as an evaporator of the heat pump. The refrigerant enters the solar section, and it is evaporated by collected solar energy. Then, the refrigerant goes to the compressor at gas phase and its pressure and temperature increase. High temperature working fluid condenses in the heat exchanger, later its pressure and temperature are reduced by the expansion valve. The expansion valve controls the temperature and flow

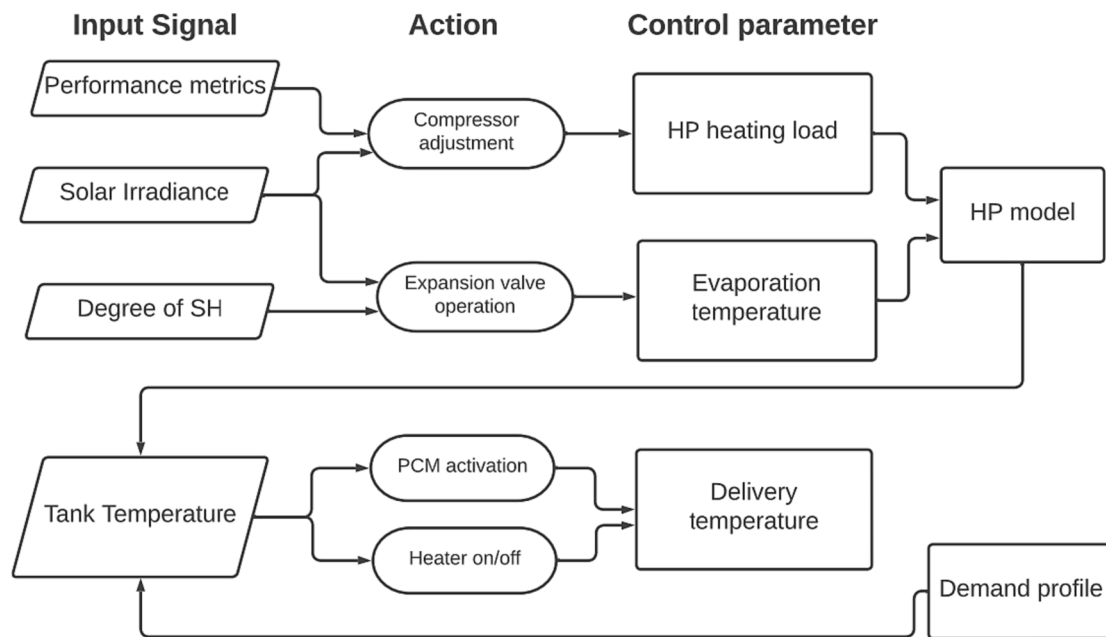


Fig. 3. Control parameters in the simulation.

rate considering the available solar energy and the collector's thermal efficiency. Fig. 1 shows the schematic of the unit.

Methodology of the paper covers PCM charging and load shifting, load management and control parameters of DX-SAHP coupled with crystallisation controllable supercooled PCM storage tank. The control parameters are delivery temperature, heat pump heating load and adjustment of evaporation temperature.

The PCM charging process is limited to solar hours since the heat pump can only operate during this period. As a result, the system enforces load shifting from peak times to daytime, aligning with solar energy availability. The DX-SAHP utilizes solar energy as a heat source and efficiently delivers high-temperature heat to the condenser heat exchanger. This heat is then transferred to the hot water loop, connected to the PCM storage tank, where the circulated water heats the PCM tubes. During PCM charging, the water temperature in the tank remains sufficiently high, enabling continued space heating.

Regarding the load management, the system aims to achieve optimal load management during the charging and discharging phases of the PCM storage tank. When charging is completed, the water temperature in the tank reaches approximately 70 °C, and the PCM temperature rises to more than 58 °C. This stored heat can be utilized during evening peak hours without any additional electricity consumption. However, as heating continues during the night, the tank temperature gradually decreases. To address this, the PCM tubes can be activated to increase the water supply temperature. The latent heat of the PCM provides the necessary heat to cover the early morning peak load, ensuring efficient use of stored energy. Fig. 2 shows the system operation for a given heating load and solar irradiance profile.

In order to operate the system effectively, specific control parameters and actions are determined based on the simulation results. The study introduces three different control parameters and actions, reflecting its contribution to the field:

2.1. Delivery temperature

One of the primary targets of the system is to supply the building with sufficient hot water temperature. The designed supply temperature takes into account various factors such as location, building insulation, and radiator size. The radiator design temperature can be regulated by authorities and also based on the design power of the radiator, but in the

new buildings or renovated old buildings, the supply temperature or the number of radiators is reduced in order to avoid overheating as the heating demand is lesser [33,34]. Jangsten et al., [33] presented the results of a survey of 109 radiator systems as part of a district heating system in Sweden, and they observed that ambient temperature is the main influencing factor of the supply temperature. They showed that average supply temperature is 64 °C when the outdoor temperature is -16 °C and 55 °C when the outdoor temperature is 5 °C. Regarding air to water heat pump system, Huchtemann et al., [35] used 35 °C, 45 °C and 50 °C supply temperatures to optimise the domestic heat pump system. Literature shows that air to water heat pump systems usually provide supply hot water temperature of 36 °C to 55 °C to the radiators [36–38].

2.2. Heat pump heating load and evaporation temperature

DX-SAHP systems have better performance potential compared to indirect solar-assisted pump systems and air-source heat pump systems. This better performance comes from the higher evaporation temperature with the help of the solar heat input and less heat loss because there is no additional heat exchanger and storage medium. However, the heat output of the DX-SAHP is depending on the solar intensity which directly affects the system operation. In order to provide constant heat output from the heat pump, the evaporator/solar collector needs to collect a certain amount of heat. For this reason, the evaporation temperature of the refrigerant in the collector should be adjusted. In this way, the collected heat can be secured but the heat pump performance would be affected. Therefore, the system operation should be optimised/regulated by external control strategies to maintain the operation in an acceptable range and to be sure of the daily heating demand is provided. Fig. 3 shows the adopted control mechanisms in the simulation.

If the hot water delivery temperature falls below the set temperature and the operation period allows, the PCM activation increases the tank temperature. Additionally, an electrical water heater is incorporated in the system to ensure that the water delivery temperature never falls below the set value. The simulation uses predetermined solar irradiation-heating load variations to establish the relationship between collector efficiency, heat pump performance, and heating loads based on solar intensity.

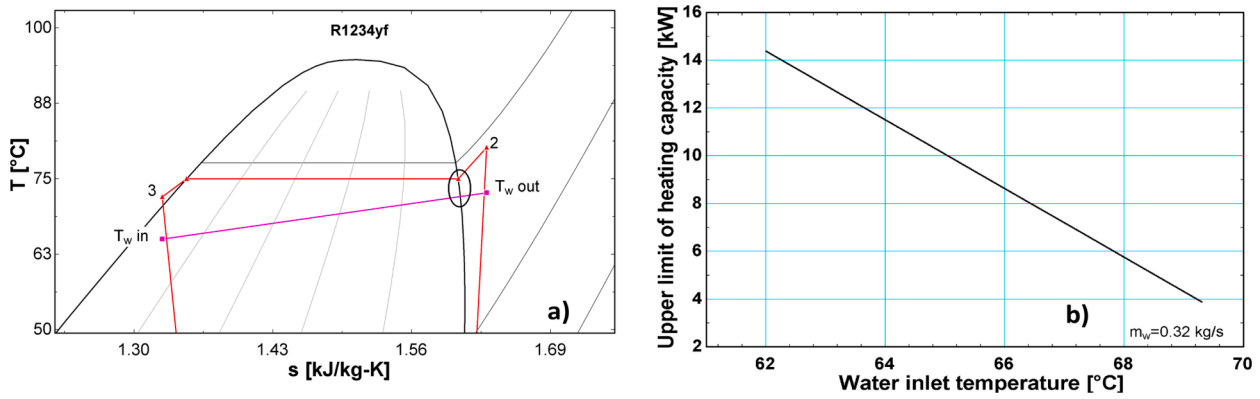


Fig. 4. A) Pinch temperature difference on T-s diagram and b) upper limit of the heating capacity for different inlet temperatures.

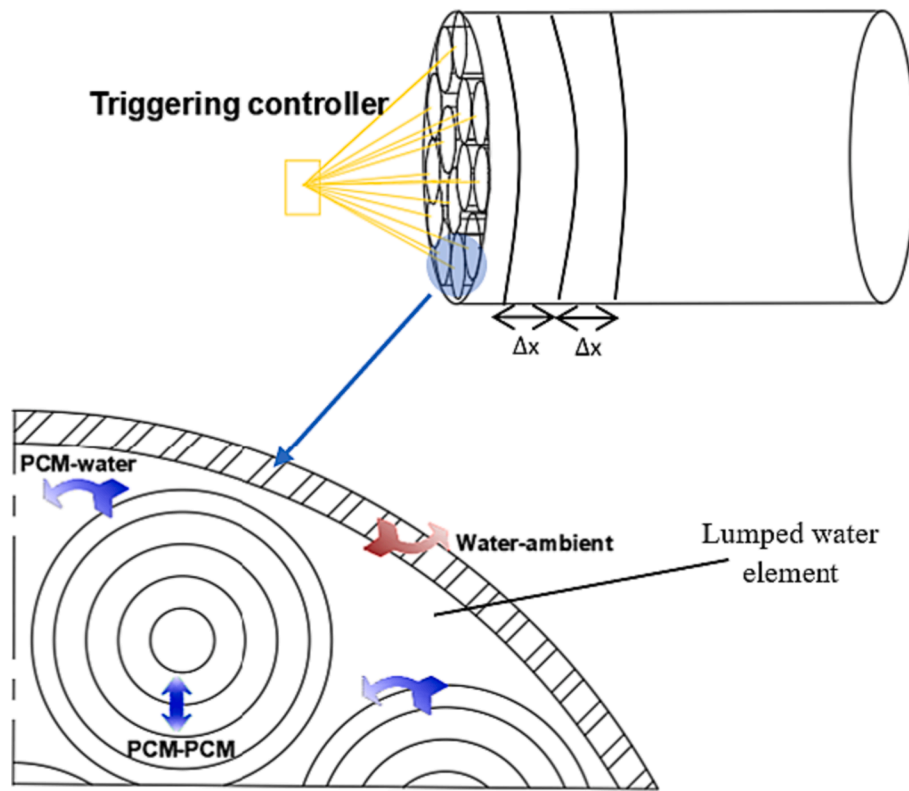


Fig. 5. PCM storage tank layout and heat transfer diagram inside the tank [29].

3. Component models of the system

3.1. Solar collectors

There is an interest in using bare solar collectors in DX-SAHP applications in the literature as bare solar collectors can operate even at night as they can harvest heat from the air as well. However, their thermal efficiencies are lower due to the heat loss. In this study, evacuated tube solar collectors are adopted to benefit low solar irradiance values with better efficiency and force the system to operate only during day times. The collector model is built on the thermal efficiency equation by neglecting thermal capacity [39]. It is clear to say that direct steam generation collectors' thermal efficiency is higher than the single-phase collectors because the convection heat transfer coefficient is better when phase change is happened [40], however, in this application, a conservative approach was applied in order to present the potential of the system. Eq. (1) is the collector thermal efficiency equation.

$$\eta_{col} = \eta_0 - c_1 \frac{\bar{T} - T_{am}}{G} - c_2 \frac{(\bar{T} - T_{am})^2}{G} \quad (1)$$

The thermal efficiency equation uses mean working fluid temperature but, in this application, the working fluid will be at constant temperature as it is at two-phase region. Where η_0 , c_1 , \bar{T} , T_{am} and G are zero-loss efficiency, collector heat loss coefficient, refrigerant evaporation temperature, ambient temperature, and solar irradiance, respectively. The modification if the efficiencies were taken from Freeman et al., [39]. The used parameters are $\eta_0 = 0.556$, $c_1 = 0.888$, $c_2 = 0.006$. The given parameters are for Thermomax HP-200 evacuated-tube heat pipe collector [41]. Eq. (2) can be used for heat balance of the collector considering absorbed heat by the collectors and the refrigerant.

$$\dot{Q}_{col} = \eta_{col} \cdot A_{col} \cdot G = \dot{m}_r \cdot (h_{col,out} - h_{col,in}) \quad (2)$$

Where A_{col} is collector area and \dot{m}_r is refrigerant mass flow rate, $h_{col,out}$

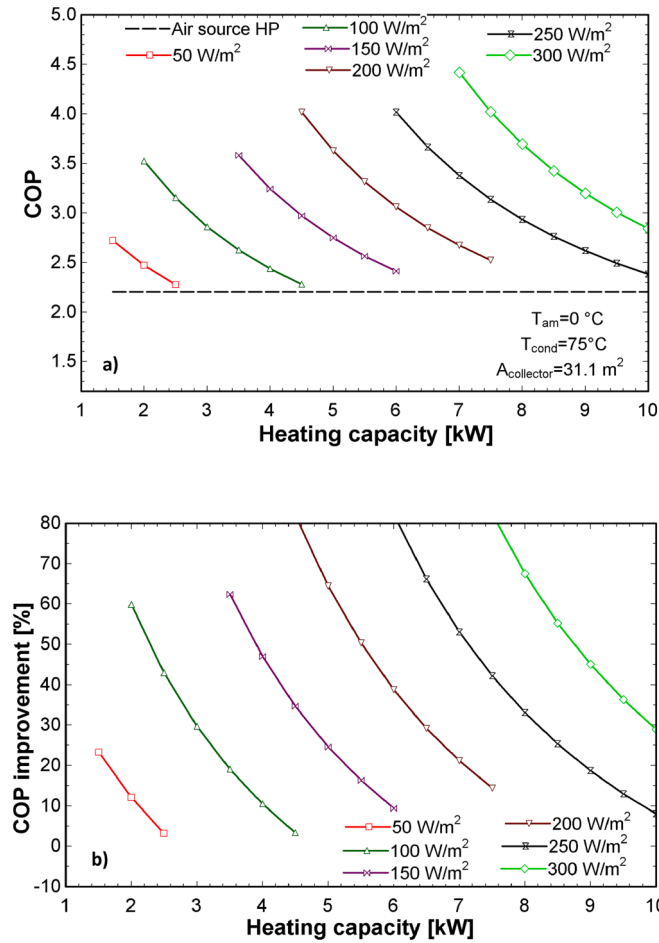


Fig. 6. Effect of solar irradiance and heating capacity on a) COP and b) COP improvement.

and $h_{col,in}$ are enthalpies of the refrigerant at collector out and inlet, respectively. Refrigerant pressure will be controlled for finding the required collector thermal efficiency to match the energy balance.

3.2. Heat pump

The heat pump consists of a compressor, a condenser, an expansion valve and an evaporator as main components. In DX-SAHP, the evaporator is solar collector where the heat is absorbed. It is assumed that the refrigerant has 3 K superheating at the collector outlet [42] and 3 K pinch temperature difference with hot water in the condenser heat exchanger. Fig. 4a shows T-s diagram for condenser pinch temperature for condensation temperature of 75 °C and water inlet temperature of 65 °C. By using this approach, the hot water outlet temperature would be 72 °C to 73 °C for various heating loads as the water flow rate is constant at 0.32 kg/s. Therefore, while providing maximum hot water temperature, the heating capacity varies as the temperature increment is limited with this approach as seen in Fig. 4b. In conclusion, regardless of the solar irradiance input, heating capacity is limited depending on water inlet temperature.

After the condenser heat exchanger, the refrigerant enters the expansion valve and isenthalpic expansion occurs. Regarding the compressor model, isentropic efficiency is considered. As the evaporation temperature depends on solar profile and heating load and condensation temperature depends on the hot water temperature, the pressure ratio of the system varies with the operating conditions. Eq. (3) is given for isentropic efficiency of the compressor for different pressure ratios [43]:

$$\eta_{is} = 0.874 - 0.0135 \cdot \frac{P_{dis}}{P_{suc}} \quad (3)$$

The COP of the heat pump can be defined in Eq. (4):

$$COP = \frac{\dot{Q}_{cond}}{\dot{W}_{comp}} \quad (4)$$

Similarly, the air source heat pump is also modelled to compare the performances. The only difference in air source heat pump is evaporator uses ambient air as a heat source. That means, the evaporation temperature depends on ambient air temperature. The difference between the evaporation temperature and the ambient air temperature is considered to be 10 °C [44] as it is recommended as a practical approach for the appropriate cost of heat exchangers [42].

For comparison of the system, COP improvement is defined in Eq.(5):

$$COP_{improvement} = \left| \frac{COP_{air} - COP}{COP_{air}} \right| * 100 \quad (5)$$

3.3. PCM storage tank

PCM storage tank is a conventional cylindrical water tank, but PCM tubes are immersed inside to enhance the heat capacity. Our previously validated PCM tank model is used in the modelling [24,29]. In the model, the PCM storage tank is divided into control volumes in a horizontal direction. For each volume, energy balance equations are considered to calculate water and PCM temperatures. Since the PCM tubes are immersed in the water, heat transfer continues during the out of heating times in discharging period. Water flow in the tank is assumed in one direction depending on the discharge side. The PCM tubes are also additionally divided into 10 radial nodes while their surrounding water is represented by one node. Fig. 5 is given to show the PCM storage tank layout. 20 PCM tubes are immersed into the water tank where the water element has contact with PCM outer surfaces and the tank wall. Based on heat transfer rates, the temperature of the water element in different horizontal nodes, PCM radial and horizontal nodes and heat loss to the ambient are calculated simultaneously.

General energy equation of PCM is used in Eq. (6) [45,46]:

$$V_{PCMj,n} \cdot \rho_{PCMj,n} \cdot L_{PCMj,n} \cdot \frac{\partial \phi_{j,n}}{\partial t} - V_{PCMj,n} \cdot \rho_{PCMj,n} \cdot c_{p,PCMj,n} \cdot \frac{\partial T_{PCMj,n}}{\partial t} = \dot{Q}_{W_n-PCMj,n} + \dot{Q}_{PCM(j-1),n-PCMj,n} + \dot{Q}_{PCMj,n-PCMj,(n+1)} \quad (6)$$

Where n is horizontal node number and j is the radial node number. $V_{PCMj,n}$ is volume of the given node, ϕ is liquid fraction of the PCM, $\rho_{PCMj,n}$ is density and $L_{PCMj,n}$ is the heat of fusion per unit mass of the PCM. $\dot{Q}_{W_n-PCMj,n}$, $\dot{Q}_{PCM(j-1),n-PCMj,n}$ and $\dot{Q}_{PCMj,n-PCMj,(n+1)}$ are convection heat transfer rate between water and the PCM element, conduction heat transfer rate between PCM nodes in the radial direction and conduction heat transfer rate between PCM nodes in horizontal direction, respectively.

For the water element, Eq.(7) is given as energy balance equation:

$$T_{w,n}(i+1) = T_{w,n}(i) + \frac{\dot{Q}_{cond,n}(i) + \dot{Q}_{loss,n}(i) + \dot{Q}_{W_n-PCMj,n}(i)}{M_{st,i} \cdot c_{p,w}} \cdot \Delta t \quad (7)$$

where $\dot{Q}_{W_n-PCMj,n}(i)$ is the heat transfer rate between PCM material and the water element.

Natural convection heat transfer equations for spherical shapes can be used to calculate the convection heat transfer coefficient for cylindrical shapes in the water tank. [47]. Nusselt number to find natural convection heat transfer coefficient is found by Eq. (8):

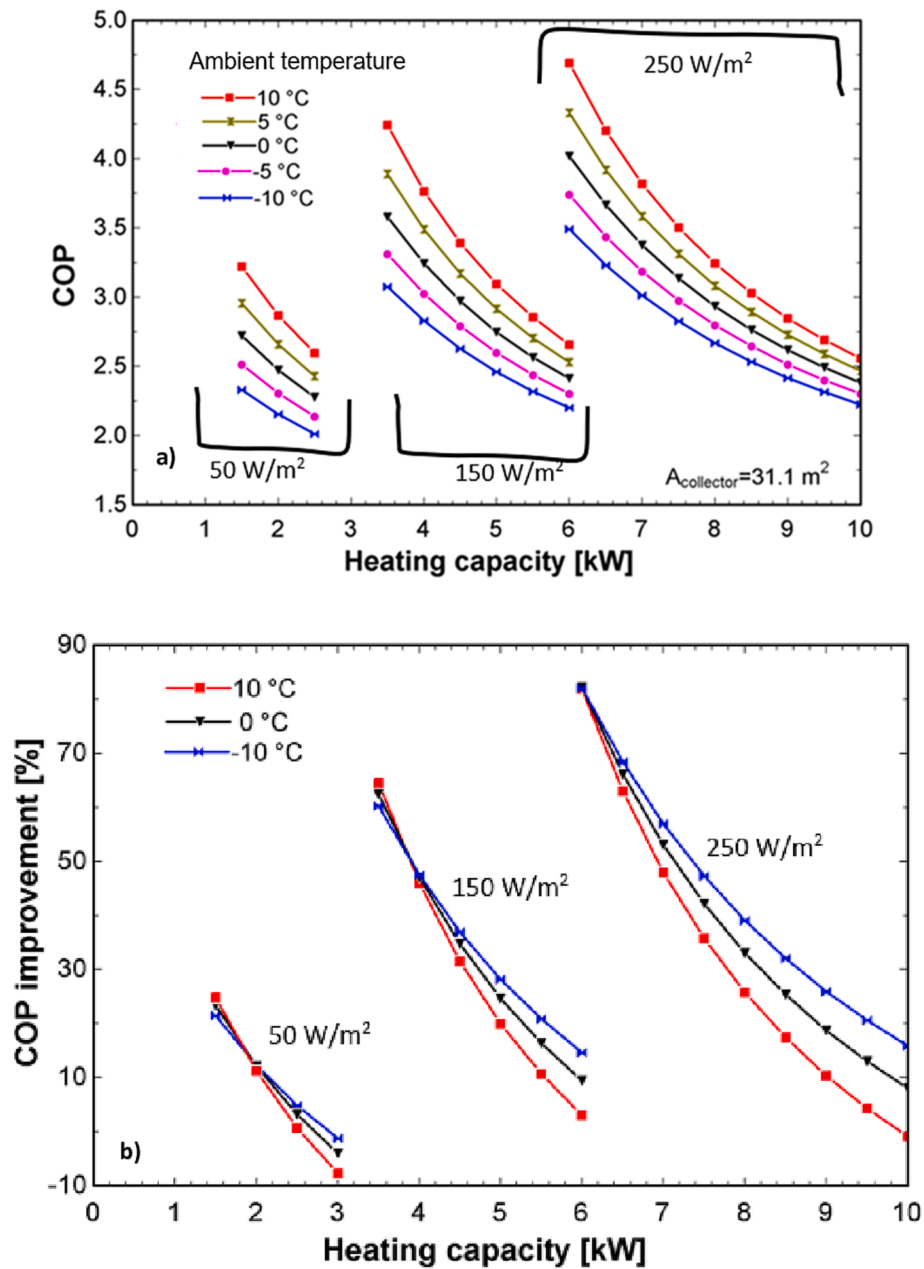


Fig. 7. Effect of solar irradiance, ambient temperature and heating capacity on a) COP and b) COP improvement.

$$Nu = \left[0.825 + \frac{0.387 \cdot Ra^{1.6}}{\left[1 + (0.492/Pr)^{9/16} \right]^{8/27}} \right]^2 \quad (8)$$

The PCM storage is assumed to be placed inside the house. Thus, the heat loss from tank to the surrounding air can be still useful for space heating. The surrounding air temperature is assumed as 20 °C. To calculate the heat loss from the PCM tank, 0.8 W/(m²K) was taken as overall tank heat loss coefficient [48].

In the following section, parametric study to reveal steady state heat pump operation will be presented for different operating conditions. Once, the system operation profile is mapped, transient analysis for a designed system will be carried out for the given heating profile. This heating profile is given in Fig. 2 to show the system methodology. The heat pump heating profile is taken from the datasets of the Renewable Heat Premium Payment (RHPP) trial [49]. The RHPP scheme was administered by the UK Energy Savings Trust and Buildings Research

Establishment to run the meter installation and data collection phases of the monitoring program. The data represents a four-bedroom detached house in the UK. It is obvious that the heating profile changes with weather conditions, building age, insulation, and user profiles, however, the heating profile can be similar for many houses showing peak load trends during morning and evening. Therefore, to represent the system performance for different solar and ambient profiles, heating demand is kept constant for different scenarios.

4. Results and discussions

The results section is divided into three parts: steady-state DX-SAHP performance evaluation with varying parameters, validation of the study, and transient simulations based on established system dynamics and determined control strategies.

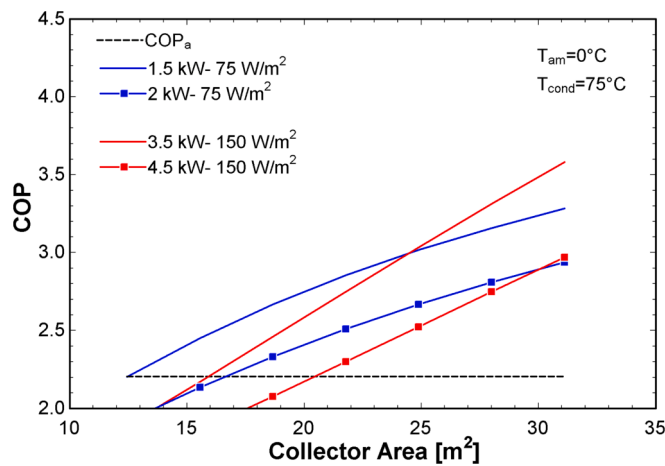


Fig. 8. Effect of solar collector area on performance for different conditions.

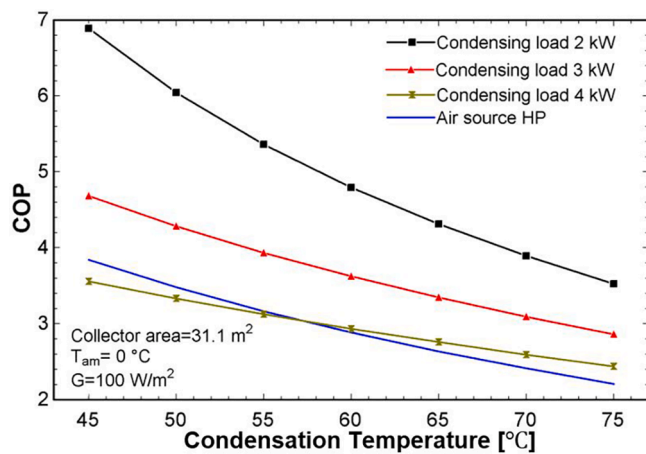


Fig. 9. COP variation for different condensation temperatures and heating capacities.

Table 1
Determined control parameters for different heating capacities and results.

Solar irradiance range W/m ²	Heating capacity kW	Evaporation temperature range	COP
0 – 74	0	–	–
75 – 99	3.5	2.68 °C – 10.64 °C	2.66 – 3.13
100 – 124	4.5	4.3 °C – 11.7 °C	2.75 – 3.2
125 – 149	7.5	–4.42 °C – 1.37 °C	2.32 – 2.6
150 – 174	8.5	–3 °C – 2.71 °C	2.4 – 2.67
175 – 199	9.5	–1.71 °C – 3.9 °C	2.46 – 2.73
200 – 299	10.5	0.22 °C – 21.57 °C	2.52 – 4
300	11	19.2 °C	3.78

4.1. Steady state calculations for DX-SAHP performance

Heating capacity is one of the important problems in DX-SAHP systems because solar irradiance varies in the day and the seasons, and it affects the heating capacity. Thus, the system should adjust its operating pressures according to solar input. Considering the collector heat absorption ability which refers to collector thermal efficiency, the heat balance equation is applied to the evaporator to find a suitable

evaporation temperature for given heating load. Fig. 6a shows the effect of solar irradiance on COP values for different heating capacities. As it is known, the condensation temperature is determined based on the water temperature that comes from the tank and changes during the day. In this analysis, the condensation temperature is chosen as 75 °C to show the lowest performance of the heat pump unit. In order to set a reference value, the COP of the air source HP is shown in the figure. When the ambient temperature is 0 °C and the condensation temperature is 75 °C, the COP of the air source HP is found 2.2 and this value remains constant regardless of the solar irradiance.

Solar irradiance value is increased by 50 W/m² for various heating capacities and COP values are obtained for given conditions. Since the collector area is constant, the amount of useful collected solar energy depends on the collector thermal efficiency and the irradiance level which was given in Eq. (2). The collector thermal efficiency directly depends on evaporation temperature; thus, the determination of the evaporation temperature is one of the indicators of the heating capacity because it affects the amount of collected heat by the collectors. Although the lower evaporation temperature collects more heat, it decreases the system performance as it increases the pressure ratio in the compressor. It can be observed from Fig. 6a that at a solar irradiance of 50 W/m², the heating capacity reaches a maximum of 2.7 kW, assuming the air source heat pump performance sets the upper limit for the given conditions. As solar irradiance values increase, the heating capacity can be an upward trend. Upon reaching a solar irradiance of 300 W/m², the DX-SAHP unit demonstrates the capability to deliver over 12 kW of heating capacity, showcasing superior performance in comparison to the air source heat pump. Fig. 6b illustrates the COP improvement of the DX-SAHP over the air source heat pump under the specified conditions. Notably, heating capacity plays a pivotal role in enhancing COP. When solar irradiance is 300 W/m², the DX-SAHP can deliver 10 kW heating with 30 % better COP compared to air source heat pump. Lower heating capacity leads to heightened performance, whereas the performance of the air source heat pump remains primarily influenced by ambient temperature, with heating capacity having no impact in this analysis.

Fig. 7 shows the effect of ambient temperature on COP and COP improvement for different solar irradiance levels. In the previous analysis, the effect of solar irradiance was shown for constant ambient temperature but in this analysis, solar irradiance is kept constant to investigate the effect of ambient temperature. It is known that ambient air temperature is the main parameter for air source HP performance, however, it also affects DX-SAHP performance.

Ambient air temperature has a positive influence on collector thermal efficiency as the higher ambient temperature means less temperature difference between the collector and ambient air which increases the thermal efficiency. Higher thermal efficiency means more useful heat can be collected by the solar collectors. In order to maintain energy balance in the collector between useful heat and refrigerant enthalpy difference, the evaporation temperature of the HP is adjusted (increased), this time, collector efficiency falls, and energy balance can be maintained for constant heating output. Higher evaporation temperature results in better HP performance. Fig. 7a is given to show the effect of ambient temperature on COP. For a constant heat output of 2 kW, when the solar irradiance is 50 W/m² and ambient temperature is –10 °C, the COP of the system is 2.15 while the air source HP COP is 1.91. When the temperature is increased to 10 °C, the COPs of DX-SAHP and air source HP are 2.86 and 2.58, respectively. For these conditions, COP improvement values are around 12 % and 11 % for –10 °C and 10 °C ambient conditions as can also be seen in Fig. 7b. However, when the heating capacity is higher, the effect of ambient temperature on COP improvement is more dominant. In Fig. 7b, the COP values go down but approach each other with higher heating capacity. However, COP improvement values diverse each other when the heating capacity is increased. When the heating capacity is 10 kW under 250 W/m² solar irradiance, COP improvement increases from 2 % to 17 % for ambient temperatures of 10 °C and –10 °C, respectively.

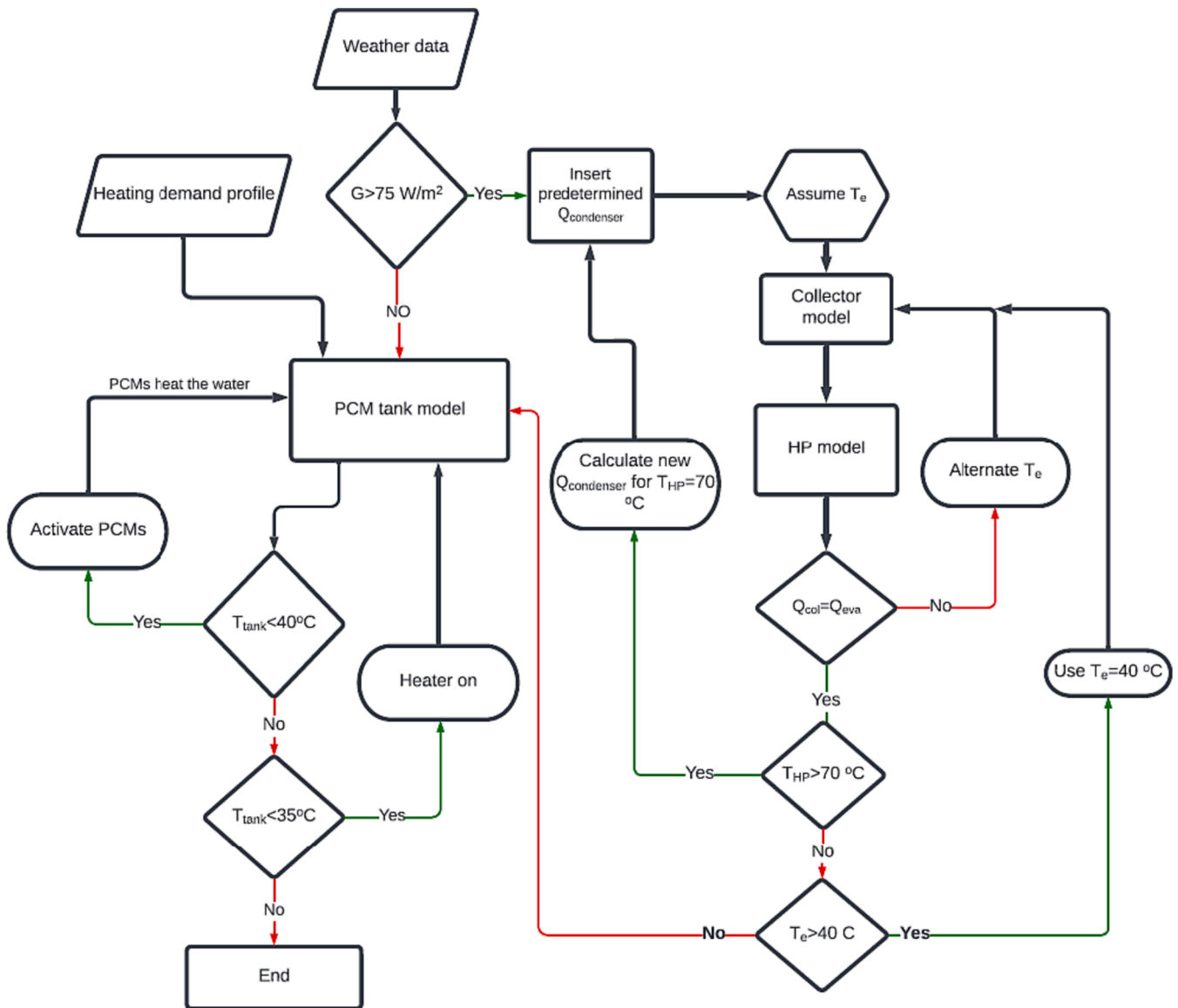


Fig. 10. Simulation flowchart of the mathematical model.

Table 2
Determined system components and specifications.

Daily heating load	46 kWh	Solar collector area	43.54 m ²
Total SAT mass in tank	113 kg	Heat Pump output	Maximum 12 kW
Total PCM volume in tank	78 L	Pinch temperature in HP condenser	3 °C
Solar collector type	Evacuated tube collectors	Flow rate between buffer tank and HP	0.33 kg/s
One PCM tube volume	3.12 L	Water mass in tank	515 kg
SAT latent heat	264 kJ/kg	Tank heat loss coefficient	0.8 W/(m ² K)
SAT conductivity	0.6/0.385 W/(mK)	SAT Specific heat	2.9/3.1 kJ/(kgK)
Tank volume	600 L	SAT density	1450 kg/m ³

After presenting the effect of heating capacity and ambient temperature, the effect of the solar collector area on COP is shown in Fig. 8. For a constant heating capacity and solar irradiance, larger collector areas increase the system’s performance. The reason is similar to the effect of

solar irradiance level which is the amount of collected solar heat. A larger collector area means more heat collection and for a constant heating output, the evaporation temperature is lifted to maintain energy balance which results in better performance. Increasing the collector area from 20 m² to 31 m² when the heating load is 4.5 kW and solar irradiance is 150 W/m², instant COP increases from 2.1 to 3.1.

Although the effect of collector area has a positive effect on performance, the system performance improvement relies on the operating conditions. The trends of the COP change are similar for the same solar irradiance values even for different heat outputs, but when the solar irradiance is changed, the trend changes. Therefore, the system performance is directly related to the operating parameters as the system operation is controlled by given parameters.

The final parameter in the steady-state analysis is condensation temperature. The condensation temperature determines the compressor discharge pressure and has an influence on the system COP. The temperature depends on the heat sink temperature, it is circulating water from the PCM storage tank. In daily operations, PCM tank temperature changes as the tank exposes charging, discharging and user controlled PCM triggering. Based on the pinch temperature difference analysis referring to Fig. 4, condensation temperature is calculated. Its effect on

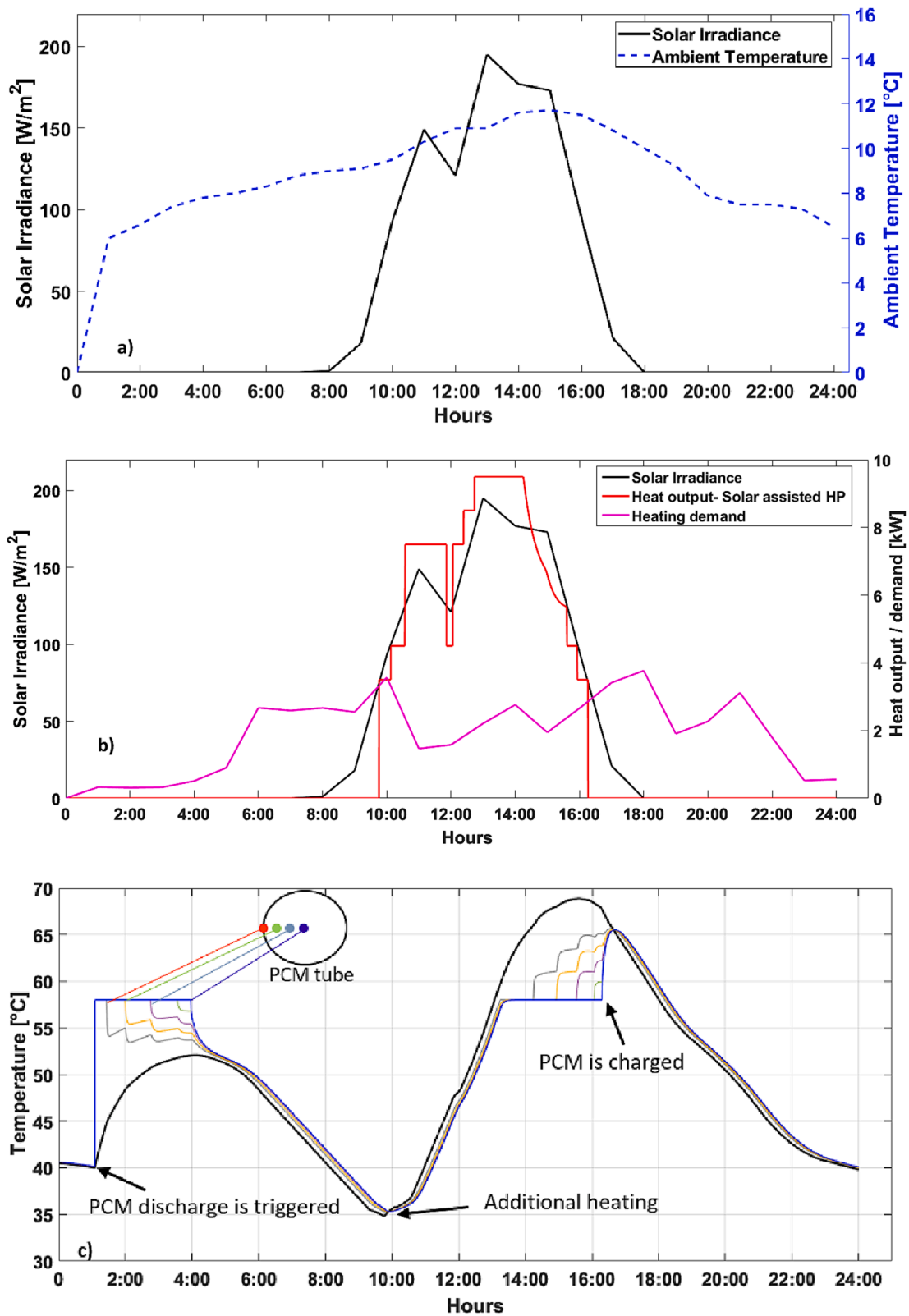


Fig. 11. a) Weather data of the low solar irradiance day, b) Heating profiles, c) Water delivery temperature and PCM triggering, d) Electricity consumption and demand shifting.

COP for different heating capacity values is given in Fig. 9. Condensation temperature has always negatively affected the performance of DX-SAHP, and air source HP as expected but the slope of the trend varies

with different heating capacities. When the condensing load is set to 4 kW, COP drops from 3.55 to 2.4 for condensation temperatures of 45 °C and 70 °C, respectively.

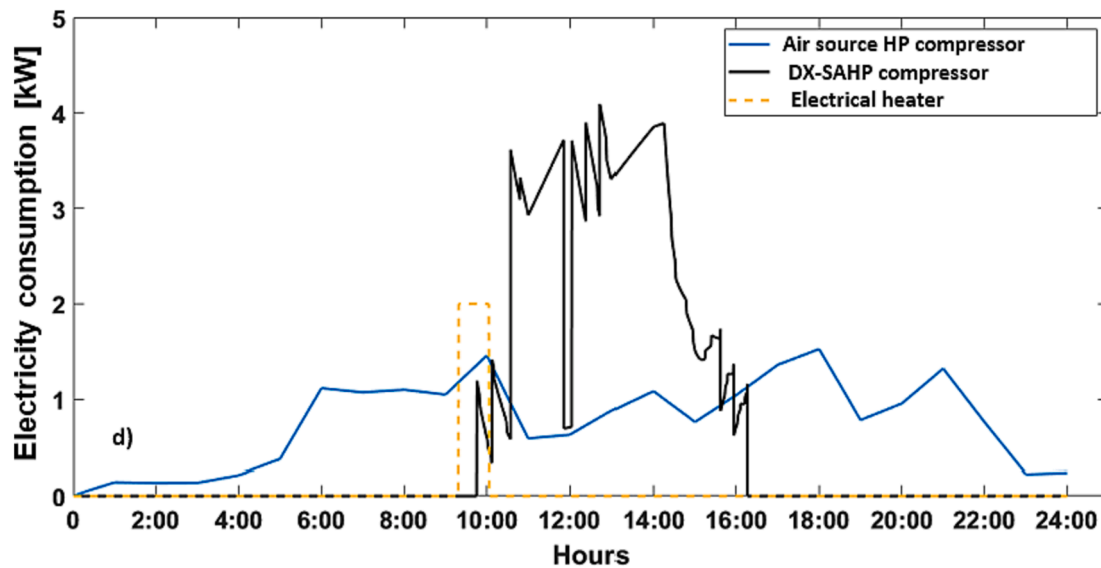


Fig. 11. (continued).

Based on the findings from the steady state analysis, in order to achieve high performance from the DX-SAHP, heating capacity needs to be adjusted for specific solar irradiance. Table 1 shows predetermined heating capacity values for different solar irradiance ranges. To show the expected performance of the unit in detail, calculated evaporation temperatures and COP values are also included for the conditions of collector area of 43.5 m^2 , condensation temperature is $75 \text{ }^\circ\text{C}$, and ambient is $0 \text{ }^\circ\text{C}$.

In real conditions, solar irradiance, ambient temperature, evaporation temperature and condensation temperature change over time and the system adapts itself to maintain operation. A flow chart is given in Fig. 10 to show how the mathematical model was built in MATLAB. Considering the predetermined heating capacity of the heat pump and considering controlled parameters, the simulation runs using real weather data and the heating demand profile of the house. The simulation starts with importing the weather data, if the solar irradiance is lower than the set value, HP is off, and the model monitors the tank temperature. If the solar value is high for HP operation, the model matches with the predetermined heating load and starts alternating the assumed evaporation temperature until the energy balance is maintained. The heated circulated water temperature cannot be higher than $70 \text{ }^\circ\text{C}$, thus, the model accepts it as $70 \text{ }^\circ\text{C}$ maximum, but it reduces the heating capacity of the HP. Lower heating output causes the rise of evaporation temperature. The model also controls the evaporation temperature to a maximum of $40 \text{ }^\circ\text{C}$. After that temperature, the HP might not be useful for heating, but the model follows a conservative approach to overcome the positive effect of other assumptions.

4.2. Validation of the study

For the DX-SAHP system, an experimental study carried out by Yu et al., [31] was chosen. In the reference paper, a direct-expansion solar-assisted heat pump with evacuated tube collector-evaporator system was tested for different parameters. In the present paper, the methodology reflects the performance of the DX-SAHP system based on determined heating output values. The model calculates solar heat gain and applies energy balance to find the evaporation temperature and COP of the system. Although the performance of the vapour compression system components can be assumed, such as condenser design is matured and it would likely give close results if condensation temperature and the water temperature difference are kept $3\text{--}8 \text{ }^\circ\text{C}$, solar collector performance depends on design. Moreover, the system performance is

significantly related to the collector performance, and it should be the same collector with the reference.

In the reference paper [31], evacuated tube collector area is 1.5 m^2 , ambient temperature is $26.2 \text{ }^\circ\text{C}$, water temperature is $60 \text{ }^\circ\text{C}$ and superheating was set for $4.7 \text{ }^\circ\text{C}$. In the case, solar irradiance of 1099.98 W/m^2 and heating output of 1459.13 W were taken as input parameters. Condensation temperature is assumed as $63 \text{ }^\circ\text{C}$ which gives compressor output pressure of 1805 kPa . Calculated collector efficiency is 0.72 but the measured efficiency in the reference is 0.75 . The COP of the system is calculated 5.38 and the experimental result was 5.11 . The relative error of COP is around 5% which can be acceptable for this case. In various scenarios, such as instances with lower solar irradiance, the error tends to increase, the error is getting larger as the collectors are not identical in the model and the experiment. Because during periods of low solar irradiance, the collector design exerts a more pronounced influence on collector efficiency.

4.3. Transient simulations of the unit

In order to simulate the potential of the proposed system, 24-hour simulation for real weather conditions and building demand need to be considered. As the system is sensitive to varying conditions, transient analysis has been carried out. The main consideration of crystallisation-controllable supercooled PCM, the PCM material must be completely melted, otherwise, self-triggering might be observed, and user-controlled heat release cannot happen. Therefore, maximum heat output has been considered. The system design specifications can be summarised in Table 2.

4.4. Low solar irradiance day

This subsection analyses the performance of the system on a low solar irradiance day and discusses the system's response and energy-saving potential. The weather data is taken from the EnergyPlus weather data of Birmingham, UK [50], and represents low solar days in the UK where the maximum solar irradiance reaches 190 W/m^2 . Fig. 11a shows the selected day's ambient temperature variation and solar irradiance data. The heating demand profile from the building is given in Fig. 11b. This profile is equivalent to a daily 46 kWh heating demand and combines DHW and space heating. Fig. 11b also shows the proposed methodology of the heating output relation with solar irradiance. The heating profile successfully follows the solar profile and given control

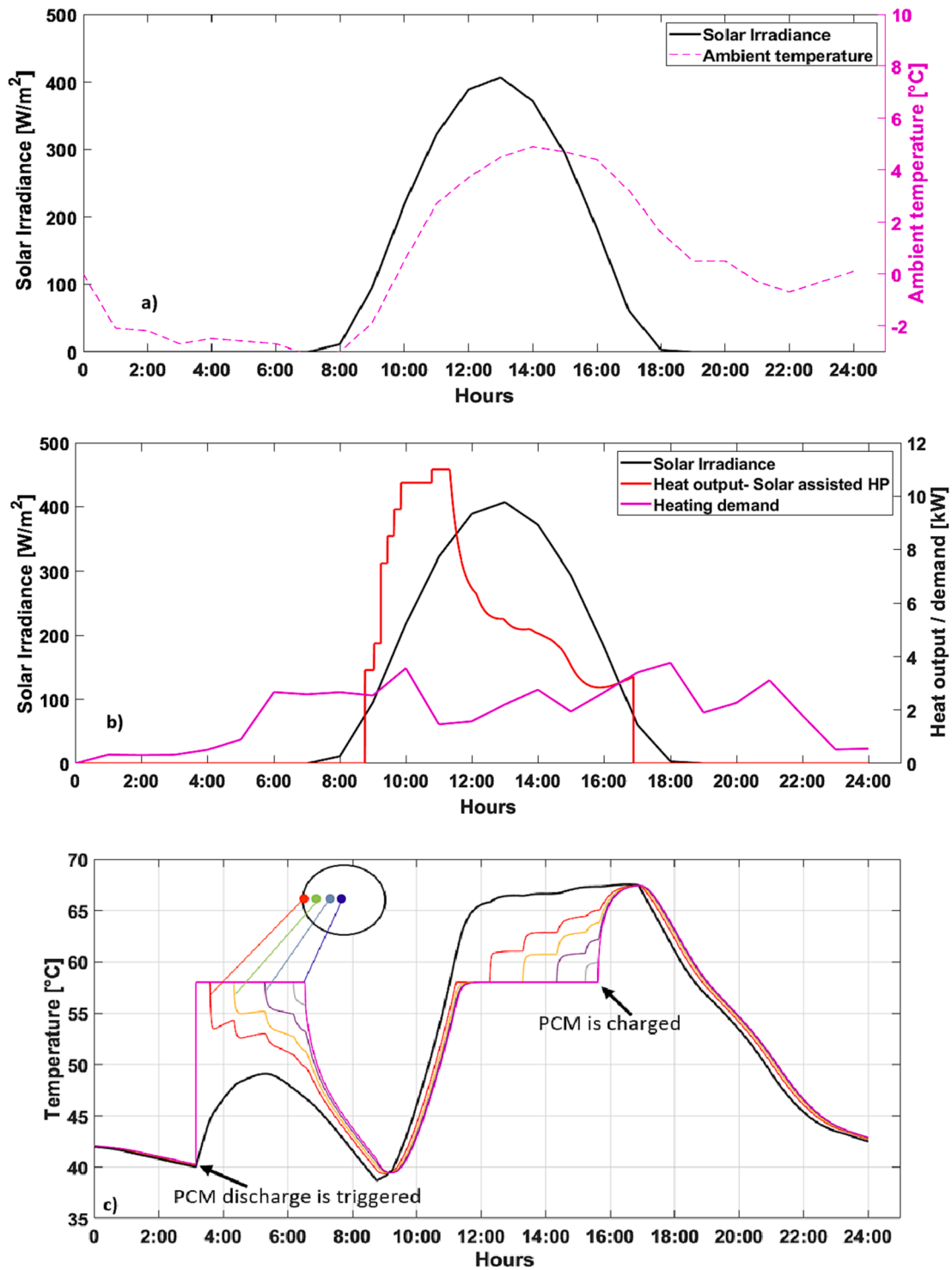


Fig. 12. a) Weather data of the high solar irradiance day, b) Heating profiles, c) Water delivery temperature and PCM triggering, d) Electricity consumption and demand shifting.

methods. At the end of the day, DX-SAHP provides a total of 45.3 kWh of heating. This value is lower than the heating demand because the designed heating profile is not enough. This is one of the renewable energy issues as the unit is designed for a low solar day, but the evaluated day is an extremely low solar day. As a result, the auxiliary electric heater was on for a period to avoid water supply temperature lower than 35 °C. Fig. 11b shows that DX-SAHP runs very well with the solar profile,

it starts operation at 9:40 and stops at 16:10. The 24-hour heating requirement was moved to the daytime when the grid load is not high. Fig. 11c shows the water delivery temperature and temperatures of the radial nodes of the PCM tube in the middle of the tank. As a control parameter, when the temperature falls to 40 °C at 1:00, PCMs are triggered and the PCM temperature rises to 58 °C. The activated PCMs heat the water tank, and the water supply temperature to the building

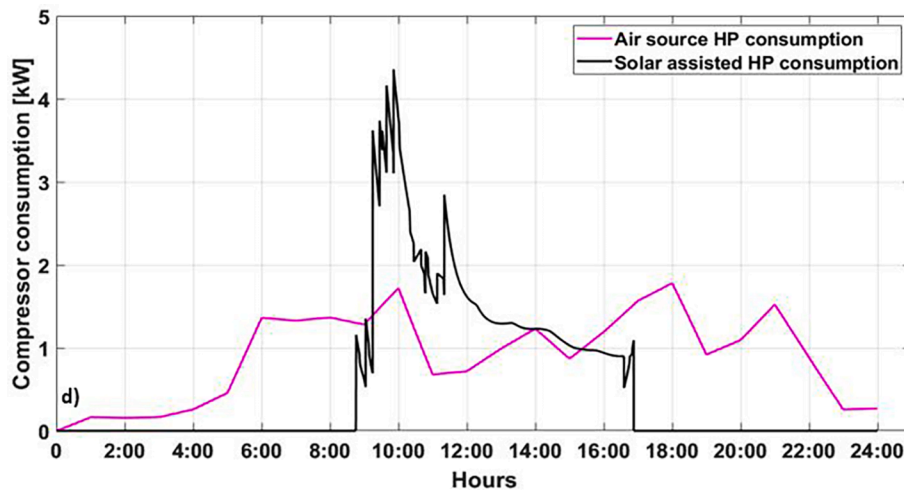


Fig. 12. (continued).

increases to 52 °C at 4:15. After that time, the temperature in the tank falls as the heating demand increases. At 9:20, the electric heater is switched on for 45 min until the temperature of the tank starts to increase. With the running of the DX-SAHP, the tank temperature increases, and at the same time, the PCM temperature increases as well. PCM sensible heating continues until 13:00, then charging starts. PCMs are totally melted at 16:20, which means PCMs are ready for triggering the next time. Around the same time, DX-SAHP switched off, and the tank temperature starts to decrease again because of the building heating demand. Fig. 11d shows the electricity consumption of the DX-SAHP, the alternative heating system air source HP, and the auxiliary heating unit for 45 min in the morning. As the system shifts the electric consumption to the daytime, electricity load is higher than the air source HP consumption. For the given day operation, DX-SAHP consumption is 16 kWh and the electric heater is 1.45 kWh, while air source HP is 18.84 kWh. The daily COP of the air source HP system is found to be 2.44, including the electricity consumption of heating, and DX-SAHP COP is found to be 2.67. The performance improvement is only 9.4 % and the system still saves 1.4 kWh of electricity compared to the conventional HP system on this low solar day.

4.5. High solar irradiance day

In order to show the advantage of using DX-SAHP, high solar irradiance day is chosen for this subsection. Fig. 12a shows weather data of the high solar irradiance day and ambient temperature of the day. The ambient temperature is lower on this day as the sky is clear, despite it is a colder day, the heating demand of the building is kept the same to obtain the system's performance for the same heating load. On this day, solar irradiance reaches 400 W/m² which enables the HP operation for maximum heating output. Fig. 12b shows heating demand, solar irradiance and DX-SAHP heat output profiles. The heating output of the HP follows the solar profile as predetermined previously. When solar irradiance reaches 300 W/m² at 11:00, the heating output is 11 kW, however, heating output decreases despite the solar irradiance increases. The reason for this reduction is related to HP's high-temperature limit. As the heat pump condensation temperature is fixed at 75 °C, the heating rate is limited considering the heat transfer rate and heat exchanger performance. Therefore, heating capacity decreases. It results in a higher evaporation temperature of the refrigerant. But evaporation temperature is also limited to maintain the operational pressure difference range of the compressor. Thus, some solar energy is wasted as the tank cannot extract additional heat from the HP. Fig. 12c shows the hot water supply temperature and PCM activation times. Since 40 °C is the set temperature to trigger the PCM, at 3:00 the PCM is triggered and the

water temperature in the tank increases. At 6:40, the PCMs have already discharged all stored heat and follow a similar temperature trend with hot water. DX-SAHP heats the water tank and PCM charging is completed at 15:40. Fig. 12d shows the electricity consumption of DX-SAHP and air source HP. In this case, the auxiliary electric heater was not used. Electricity load from the grid is moved to daytime with DX-SAHP but the power rate is increased as expected. DX-SAHP provided 49.2 kWh of heating and compressor energy consumption is found 10.1 kWh. On the other hand, air source HP consumption reaches 20 kWh because the ambient air temperature is lower. Daily COP values are calculated as 4.07 and 2.3 for DX-SAHP and air source HP, respectively.

The system's operation with solar profile and heating output relation worked very well when the solar irradiance profile is weak because the collector size is large enough to utilise the solar energy even under low solar irradiance. The relationship between solar irradiance and HP heating capacity has been modelled and controlled for large collector areas where the solar energy is low. In high solar irradiance day operation, the same collector area converts more solar energy to useful energy and heats the PCM storage faster than low solar profile day. As can be seen from Fig. 12b, the heat output profile could match the solar profile in a better way because the system didn't reflect its potential very well. The unit could heat the water slowly and could benefit from the high solar energy in the middle of the day with more efficiency and heating capacity. Therefore, the system does not operate at optimum performance but provides sufficient heating with better performance than conventional HP.

4.6. Transient simulation for one month

Although the low and high solar irradiance days are indicators of the system's performance, a longer time of operation is necessary. For this purpose, a one-month simulation is conducted using real weather data of Birmingham from the 15th of February to the 15th of March. The weather data is given in Fig. 13a. Although the solar profile fluctuates during the period, except for a few days, a moderate to good solar profile is observed. As expected, the system performance is found very well as the solar radiation is good for the 31 days of operation. Fig. 13b shows the COP of the DX-SAHP and conventional air source HP values. Conventional HP COP is seen between 2.2 and 3, on the other hand, DX-SAHP COP can reach even 10. However, the instant COP values may not show the real performance of the unit because the instant COP doesn't show the heating capacity at that moment. The COP of the unit can be discussed by using one month of performance. Fig. 13c shows the electricity consumption profiles. DX-SAHP produces a total of 1463 kWh of heat with compressor consumption of 364 kWh. However, additional

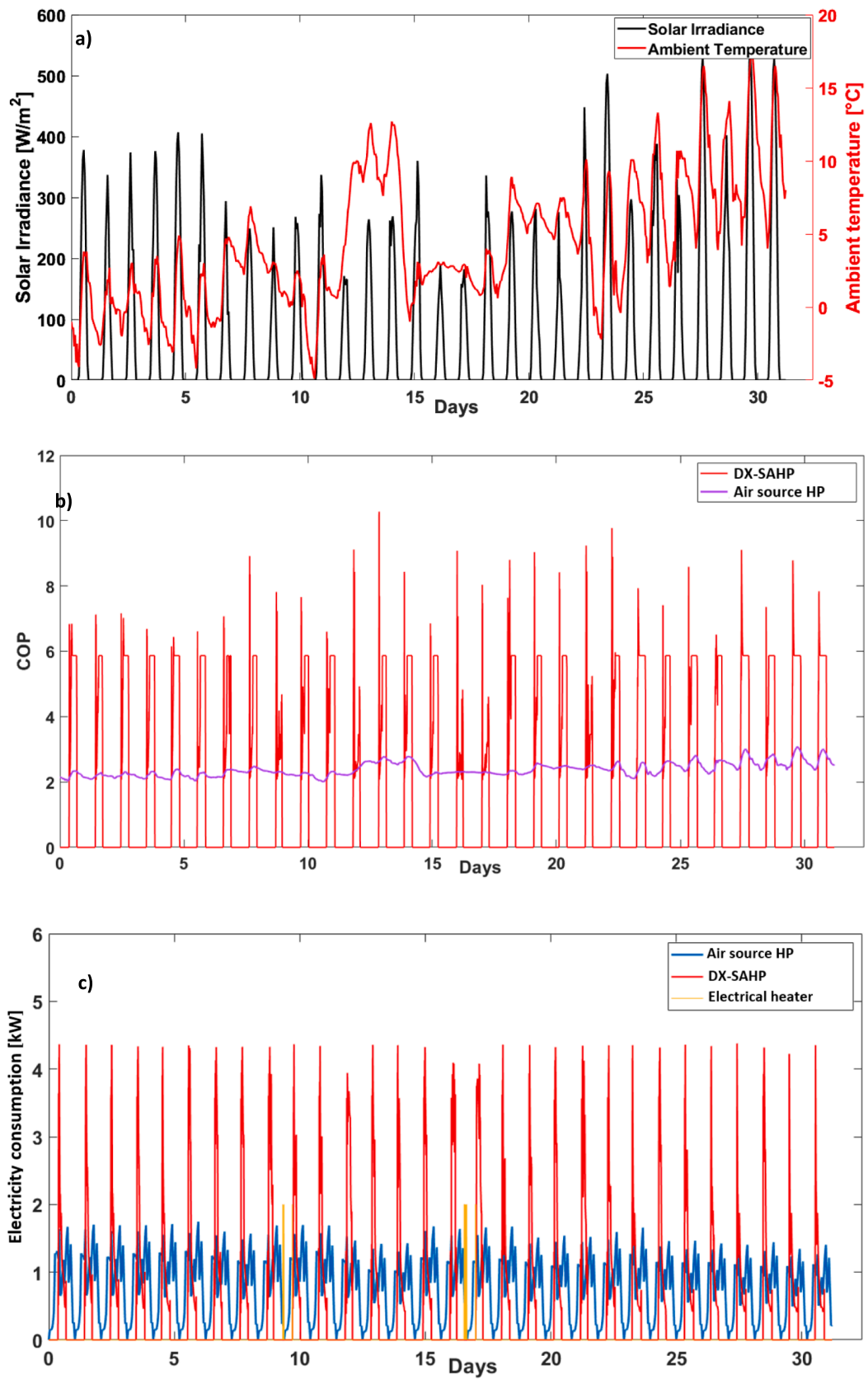


Fig. 13. A) Weather data of February, b) COP variation of both systems, c) Electricity consumptions and heating by immersion heater.

electric heating is also supplied to the system when solar energy is not enough to supply heating. The electricity consumption of the auxiliary heater is 6.1 kWh. On the other hand, the conventional air source HP produces 1360 kWh of heat with compressor consumption of 582 kWh. Overall COP of the DX-SAHP and conventional HP units are found 3.98 and 2.33, respectively.

The examined 30 days of operation shows that, DX-SAHP can increase the heating COP by around 70 % however, the system performance depends on the weather conditions and the tested month is not the coldest and lowest solar period in the UK. It still shows the potential of the system especially when the solar radiation intensity reaches up to 200 W/m².

5. Conclusions

In this paper, a DX-SAHP system using evacuated tube-type solar collectors has been presented for the first time coupled with a heat storage tank including crystallisation-controllable PCM. The DX-SAHP control strategies have been given and successfully implemented in the simulation model which covers real weather data and building heating demand. Firstly, a steady-state DX-SAHP model was given to see the effecting parameters on performance and to determine the operating conditions during the simulation days. The effect of solar irradiance, heating capacity, condensation temperature and collector area were discussed. Solar irradiance-based heating capacity control methodology was presented and applied in the simulations. Low and high solar profile days were simulated and finally, one month of operation was simulated. Based on the analysis, given conclusions are drawn as follows:

- The system performance directly depends on the collected heat by the solar collectors. Evacuated tube collectors work very well to reduce the negative effect of weather conditions such as ambient temperature and wind speed, however, the solar irradiance is the main influencer of the performance.
- Although the effect of collector area has a positive effect on performance, the system performance improvement relies on the operating conditions and determined heat outputs.
- When considering a collector area of 31 m², solar irradiance of 150 W/m², and an ambient temperature of −5 °C, the DX-SAHP achieves a COP of 2.3 while providing 6 kW of heating output. Notably, when the heating output is reduced by 1 kW, or when the ambient temperature increases to 8 °C, the system's COP demonstrates a significant increase of 13% in both scenarios.
- In low solar day, the maximum solar irradiance is less than 200 W/m², proposed DX-SAHP with control strategies and the use of controlled crystallisation PCM, can reduce the electricity consumption by 9.4 % compared to the conventional HP unit.
- In high solar day, the maximum solar irradiance reaches 400 W/m², proposed DX-SAHP with control strategies and use of controlled crystallisation PCM, the system performance is 77 % better compared to the conventional HP unit.
- For one month of operation, the overall COP of the DX-SAHP and conventional HP units were found 3.98 and 2.33, respectively.

Declaration of Competing Interest

The authors declare that they have no known competing financial interests or personal relationships that could have appeared to influence the work reported in this paper.

Data availability

The authors are unable or have chosen not to specify which data has been used.

Acknowledgements

The authors would like to acknowledge Engineering and Physical Sciences Research Council (EP/T02318X/1) for the financial support to this research.

References

- [1] M. Jakuciūnyte-Skodiene, R. Krikstolaitis, G. Liobikienė, The contribution of changes in climate-friendly behaviour, climate change concern and personal responsibility to household greenhouse gas emissions: Heating/cooling and transport activities in the European Union, *Energy* 246 (2022), <https://doi.org/10.1016/j.energy.2022.123387>.
- [2] L.F. Cabeza, M. Chàfer, Technological options and strategies towards zero energy buildings contributing to climate change mitigation: a systematic review, *Energ. Buildings* 219 (2020), <https://doi.org/10.1016/j.enbuild.2020.110009>.
- [3] Eurostat, "Energy consumption in households," 2022. https://ec.europa.eu/eurostat/statistics-explained/index.php?title=Energy_consumption_in_households (accessed Apr. 27, 2023).
- [4] M. Esen, T. Yuksel, Experimental evaluation of using various renewable energy sources for heating a greenhouse, *Energ. Buildings* 65 (2013) 340–351, <https://doi.org/10.1016/j.enbuild.2013.06.018>.
- [5] H. Esen, M. Esen, O. Ozsolak, Modelling and experimental performance analysis of solar-assisted ground source heat pump system, *J. Exp. Theor. Artif. Intell.* 29 (1) (2017) 1–17, <https://doi.org/10.1080/0952813X.2015.1056242>.
- [6] M. Esen, T. Ayhan, Development of a model compatible with solar assisted cylindrical energy storage tank and variation of stored energy with time for different phase change materials, *Energy Convers. Manag.* 37 (12) (1996) 1775–1785, [https://doi.org/10.1016/0196-8904\(96\)00035-0](https://doi.org/10.1016/0196-8904(96)00035-0).
- [7] J.G. Cervantes, E. Torres-Reyes, Experiments on a solar-assisted heat pump and an exergy analysis of the system, *Appl. Therm. Eng.* 22 (12) (2002) 1289–1297, [https://doi.org/10.1016/S1359-4311\(02\)00055-8](https://doi.org/10.1016/S1359-4311(02)00055-8).
- [8] K. Sezen, A. Gungor, Comparison of solar assisted heat pump systems for heating residences: A review, *Sol. Energy*, vol. 249, no. November 2021, pp. 424–445, 2023, doi: 10.1016/j.solener.2022.11.051.
- [9] A. Dik, C. Kutlu, S. Omer, R. Boukhanouf, Y. Su, S. Riffat, An approach for energy management of renewable energy sources using electric vehicles and heat pumps in an integrated electricity grid system, *Energ. Buildings* vol. 294, no. May (2023), 113261, <https://doi.org/10.1016/j.enbuild.2023.113261>.
- [10] T.T. Chow, G. Pei, K.F. Fong, Z. Lin, A.L.S. Chan, M. He, Modeling and application of direct-expansion solar-assisted heat pump for water heating in subtropical Hong Kong, *Appl. Energy* 87 (2) (2010) 643–649, <https://doi.org/10.1016/j.apenergy.2009.05.036>.
- [11] A. Moreno-Rodriguez, N. Garcia-Hernando, A. González-Gil, M. Izquierdo, Experimental validation of a theoretical model for a direct-expansion solar-assisted heat pump applied to heating, *Energy* 60 (2013) 242–253, <https://doi.org/10.1016/j.energy.2013.08.021>.
- [12] X. Kong, X. Yan, Z. Yue, P. Zhang, Y. Li, Influence of refrigerant charge and condenser area on direct-expansion solar-assisted heat pump system for radiant floor heating, *Sol. Energy* 247 (October) (2022) 499–509, <https://doi.org/10.1016/j.solener.2022.10.051>.
- [13] X.Q. Kong, Y. Li, L. Lin, Y.G. Yang, Modeling evaluation of a direct-expansion solar-assisted heat pump water heater using R410, *Int. J. Refrig* 76 (2017) 136–146, <https://doi.org/10.1016/j.ijrefrig.2017.01.020>.
- [14] X. Kong, K. Jiang, S. Dong, Y. Li, J. Li, Control strategy and experimental analysis of a direct-expansion solar-assisted heat pump water heater with R134a, *Energy* 145 (2018) 17–24, <https://doi.org/10.1016/j.energy.2017.12.114>.
- [15] S.N. Rabelo, T.F. Paulino, W.M. Duarte, A.A.T. Maia, L. Machado, Experimental analysis of the influence of the expansion valve opening on the performance of the small size CO₂ solar assisted heat pump, *Sol. Energy* 190 (May) (2019) 255–263, <https://doi.org/10.1016/j.solener.2019.08.013>.
- [16] S.N. Rabelo, T.F. Paulino, C.P.M. Soares, W.M. Duarte, L. Machado, R.O. Nunes, Mass flow characteristics of CO₂ operating in a transcritical cycle flowing through a needle expansion valve in a direct-expansion solar assisted heat pump, *J. Build. Eng.*, vol. 67, no. November 2022, p. 105963, 2023, doi: 10.1016/j.jobe.2023.105963.
- [17] P. Yin, X. Kong, Z. Yue, H. Yu, Y. Li, J. Li, Evaporation temperature prediction of a direct-expansion solar-assisted heat pump, *Sol. Energy* 256 (March) (2023) 215–224, <https://doi.org/10.1016/j.solener.2023.03.052>.
- [18] L.F. Cabeza, et al., CO₂ mitigation accounting for thermal energy storage (TES) case studies, *Appl. Energy* 155 (2015) 365–377, <https://doi.org/10.1016/j.apenergy.2015.05.121>.
- [19] M. Esen, Thermal performance of a solar-aided latent heat store used for space heating by heat pump, *Sol. Energy* 69 (1) (2000) 15–25, [https://doi.org/10.1016/S0140-6701\(01\)80659-7](https://doi.org/10.1016/S0140-6701(01)80659-7).
- [20] C. Zhu, B. Li, S. Yan, Q. Luo, C. Li, Experimental research on solar phase change heat storage evaporative heat pump system, *Energy Convers. Manag.*, vol. 229, no. November 2020, p. 113683, 2021, doi: 10.1016/j.enconman.2020.113683.
- [21] T. Xu, E.N. Humire, J.N. Chiu, S. Sawalha, Latent heat storage integration into heat pump based heating systems for energy-efficient load shifting, *Energy Convers. Manag.* 236 (2021), 114042, <https://doi.org/10.1016/j.enconman.2021.114042>.
- [22] C. Kutlu, Y. Zhang, T. Elmer, Y. Su, S. Riffat, A simulation study on performance improvement of solar assisted heat pump hot water system by novel controllable

- crystallization of supercooled PCMs, *Renew. Energy* 152 (2020) 601–612, <https://doi.org/10.1016/j.renene.2020.01.090>.
- [23] H.M. Teamah, M.F. Lightstone, Numerical study of the electrical load shift capability of a ground source heat pump system with phase change thermal storage, *Energ. Buildings* 199 (2019) 235–246, <https://doi.org/10.1016/j.enbuild.2019.06.056>.
- [24] C. Kutlu, et al., Incorporation of controllable supercooled phase change material heat storage with a solar assisted heat pump: Testing of crystallization triggering and heating demand-based modelling study, *J. Energy Storage* vol. 55, no. PD (2022), 105744, <https://doi.org/10.1016/j.est.2022.105744>.
- [25] G. Wang, et al., Review on sodium acetate trihydrate in flexible thermal energy storages: properties, challenges and applications, *J. Energy Storage* vol. 40, no. May (2021), 102780, <https://doi.org/10.1016/j.est.2021.102780>.
- [26] G. Englmair, C. Moser, S. Furbo, M. Dannemand, J. Fan, Design and functionality of a segmented heat-storage prototype utilizing stable supercooling of sodium acetate trihydrate in a solar heating system, *Appl. Energy*, vol. 221, no. November 2017, pp. 522–534, 2018, doi: 10.1016/j.apenergy.2018.03.124.
- [27] G. Englmair, et al., Crystallization by local cooling of supercooled sodium acetate trihydrate composites for long-term heat storage, *Energ. Buildings* 180 (2018) 159–171, <https://doi.org/10.1016/j.enbuild.2018.09.035>.
- [28] C. Dong, R. Qi, H. Yu, L. Zhang, Electrically-controlled crystallization of supercooled sodium acetate trihydrate solution, *Energ. Buildings* 260 (2022), 111948, <https://doi.org/10.1016/j.enbuild.2022.111948>.
- [29] C. Kutlu, Y. Su, Q. Lyu, S. Riffat, Thermal management of using crystallization-controllable supercooled PCM in space heating applications for different heating profiles in the UK, *Renew. Energy* 206 (January) (2023) 848–857, <https://doi.org/10.1016/j.renene.2023.02.077>.
- [30] R. Hirmiz, H.M. Teamah, M.F. Lightstone, J.S. Cotton, Performance of heat pump integrated phase change material thermal storage for electric load shifting in building demand side management, *Energ. Buildings* 190 (2019) 103–118, <https://doi.org/10.1016/j.enbuild.2019.02.026>.
- [31] X. Yu, Z. Guo, Z. Gao, B. Yang, X. Ma, S. Dong, Thermodynamic investigation of a direct-expansion solar assisted heat pump with evacuated tube collector-evaporator, *Renew. Energy* 206 (January) (2023) 418–427, <https://doi.org/10.1016/j.renene.2023.01.112>.
- [32] S. Tangwe, P. Mukumba, G. Makaka, An installed hybrid direct expansion solar assisted heat pump water heater to monitor and modeled the energy factor of a university students' accommodation, *Energies* 16 (3) (2023) pp, <https://doi.org/10.3390/en16031159>.
- [33] M. Jangsten, J. Kensby, J.O. Dalenbäck, A. Trüschel, Survey of radiator temperatures in buildings supplied by district heating, *Energy* 137 (2017) 292–301, <https://doi.org/10.1016/j.energy.2017.07.017>.
- [34] P. Lauenburg, J. Wollerstrand, Adaptive control of radiator systems for a lowest possible district heating return temperature, *Energ. Buildings* 72 (2014) 132–140, <https://doi.org/10.1016/j.enbuild.2013.12.011>.
- [35] K. Huchtemann, D. Müller, Simulation study on supply temperature optimization in domestic heat pump systems, *Build. Environ.* 59 (2013) 327–335, <https://doi.org/10.1016/j.buildenv.2012.08.030>.
- [36] M. Dongellini, G.L. Morini, On-off cycling losses of reversible air-to-water heat pump systems as a function of the unit power modulation capacity, *Energy Convers. Manag.* 196 (March) (2019) 966–978, <https://doi.org/10.1016/j.enconman.2019.06.022>.
- [37] H. Li, et al., Impact of water volume on the energy saving potential of air source heat pump systems, *Int. J. Refrig* 130 (2021) 128–139, <https://doi.org/10.1016/j.jrefrig.2021.06.025>.
- [38] P. Conti, A. Franco, C. Bartoli, D. Testi, A design methodology for thermal storages in heat pump systems to reduce partial-load losses, *Appl. Therm. Eng.*, vol. 215, no. November 2021, p. 118971, 2022, doi: 10.1016/j.applthermaleng.2022.118971.
- [39] J. Freeman, I. Guarracino, S.A. Kalogirou, C.N. Markides, A small-scale solar organic Rankine cycle combined heat and power system with integrated thermal energy storage, *Appl. Therm. Eng.* 127 (2017) 1543–1554, <https://doi.org/10.1016/j.applthermaleng.2017.07.163>.
- [40] D. Gao, J. Li, X. Ren, T. Hu, G. Pei, A novel direct steam generation system based on the high-vacuum insulated flat plate solar collector, *Renew. Energy* 197 (June) (2022) 966–977, <https://doi.org/10.1016/j.renene.2022.07.102>.
- [41] Kingspan, Direct flow vacuum tube solar collector, 2017. .
- [42] G.F. Hundy, *Refrigeration, Air Conditioning and Heat Pumps*, 5th ed., Butterworth-Heinemann, 2016.
- [43] O. Brunin, M. Feidt, B. Hivet, Comparison of the working domains of some compression heat pumps and a compression-absorption heat pump, *Int. J. Refrig* 20 (5) (1997) 308–318, [https://doi.org/10.1016/S0140-7007\(97\)00025-X](https://doi.org/10.1016/S0140-7007(97)00025-X).
- [44] C. Kutlu, M. Tahir, J. Li, Y. Wang, Y. Su, A study on heat storage sizing and flow control for a domestic scale solar-powered organic Rankine cycle-vapour compression refrigeration system, *Renew. Energy* 143 (2019) 301–312, <https://doi.org/10.1016/j.renene.2019.05.017>.
- [45] G. Manfrida, R. Secchi, K. Stańczyk, Modelling and simulation of phase change material latent heat storages applied to a solar-powered Organic Rankine Cycle, *Appl. Energy* 179 (2016) 378–388, <https://doi.org/10.1016/j.apenergy.2016.06.135>.
- [46] J. Riffat, C. Kutlu, E.T. Brito, Y. Su, S. Riffat, Performance analysis of a pv powered variable speed dc fridge integrated with pcm for weak/off-grid setting areas, *Futur. Cities Environ.* 7 (1) (2021) 1–18, <https://doi.org/10.5334/fce.121>.
- [47] R. Padovan, M. Manzan, Genetic optimization of a PCM enhanced storage tank for solar domestic hot water systems, *Sol. Energy* 103 (2014) 563–573, <https://doi.org/10.1016/j.solener.2013.12.034>.
- [48] E. Bellos, C. Tzivanidis, C. Symeou, K.A. Antonopoulos, Energetic, exergetic and financial evaluation of a solar driven absorption chiller – a dynamic approach, *Energy Convers. Manag.* 137 (2017) 34–48, <https://doi.org/10.1016/j.enconman.2017.01.041>.
- [49] R. Lowe, Department of energy and climate change, renewable heat premium payment scheme: heat pump monitoring: cleaned data, 2013–2015. [data collection], UK Data Serv., 2017, doi: 10.5255/UKDA-SN-8151-1.
- [50] “EnergyPlus. Weather data.” <https://energyplus.net/weather/> (accessed Oct. 30, 2020).